EVALUATION OF THE THERMAL ENVIRONMENT AROUND THE HUMAN BODY IN A SOLAR RADIATION ENVIRONMENT STUDY OF COUPLED ANALYSIS OF CFD AND THERMOREGULATION MODELS

Yuta Yamane [1], Taku Ito [1], Koji Sakai[1], and Hiroki Ono [1]
[1] Meiji University, Tokyo, Japan

ABSTRACT

The purpose of this research is to evaluate the thermal environment around the human body in an environment exposed to solar radiation. First, we performed a subjective experiment in order to understand the subjective as well as the room interior's thermal environment. In this report, we include a comparison of the measurement results in order to evaluate the usefulness of including CFD analysis in the thermoregulation model. Consequently, we were able to gain an understanding of the localized thermal regulation function of the human body in a solar radiation environment by expanding the 65MN model to the surface of each component.

INTRODUCTION

In the perimeter zones of an office or in partially outside spaces such as a balcony, it is often the case that the sun creates non-uniform radiant fields. Therefore, the purpose of this research is to evaluate the thermal environment around the human body in non-uniform radiant fields. However, as an experimental method, it requires a lot of effort to change the conditions in order to assess the thermal environment on or around the human body in solar radiation fields. In contrast, a numerical analysis, compared to physical experiments, doesn't have such limitations when changing the conditions, and it allows us to comprehensively examine changes as a function of time and seasons, or various methods of screening solar radiation. In this report, we use a subjective experiment to understand the thermal environment of the subject and the test room by placing the subject in the center of the room, where solar radiation can penetrate and affect the subject's body. Then, in order to evaluate the validity of numerical analysis, the results are compared with computational fluid dynamics (CFD) coupling using the 65MN thermoregulation model and numerical body model (e.g. Tanabe et al., 2001).

SUBJECTIVE EXPERIMENT SUMMARY

The experiment with the subjective experiment ran for three days, from March 28th through the 30th, 2012, in a conference room on Meiji University Ikuta Campus, Building A, 10th floor (Kawasaki City, Tama District). Fig.1 shows the details of the Measurement Room (L4.6m ×W6.4m×H2.6m) and the condition of the louvers positioned outside the room. Fig.2 shows the details of measurement points on the wall surface and poles used to measure the indoor air temperature. Fig.3 shows the details of the placement of the subject in relation to the measurement points on the walls and poles. There were 26 measurement points set around the subject, in areas with and without solar radiation. Wall temperature, air temperature, glove temperature and the amount of solar radiation entering the room were measured between 10:00 and 18:00, and the subject's body surface temperature was measured between 15:00 and 17:00, when solar radiation was on the body. Measurements were taken once per minute wherever a thermocouple was used. Also, using a thermal camera, the subject's body temperature was

Fig.1 A Measurement Room and Outside Louver

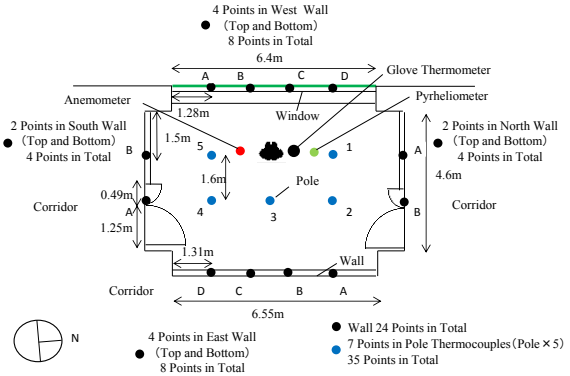

Fig.2 Plan of Measurement Room

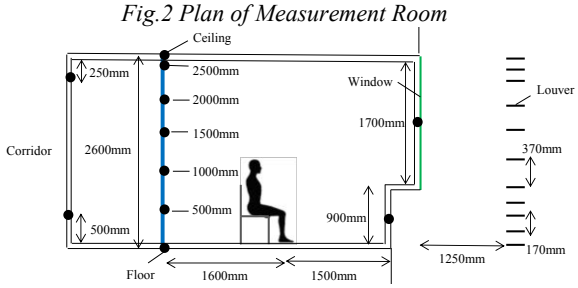

Fig.3 Elevation of Measurement Room

captured as it changed with the movement of the solar radiation. This report gives you the results on the subjective experiment from March 29th.

MEASUREMENT CONDITIONS

Fig.4 shows the glove temperature in the center of the room, the amount of indoor direct solar radiation, and the amount of outdoor horizontal solar radiation. On March 29th, the weather was sunny, and the measurements on the subjective experiment were taken between 15:30 and 16:30. The subject was wearing a long-sleeved undershirt, pants and socks. The periodical change in indoor solar radiation was caused by the outside louvers blocking the sunlight, as shown in Fig.3.

MEASUREMENT RESULTS

At 15:30, on the 29th, the surface temperature on the subject's chest and left front lower leg exceeded 35°C. At 16:00, the solar radiation began to creep into the room because, with the sun lower in the sky, the louvers failed to block all of it. Subsequently the surface temperature started to go up on the subject's front pelvis and right front lower leg. At 16:30, as the amount of solar radiation increased, it was confirmed that the overall body temperature rose. Also, the temperature was relatively high in the chest/front pelvis areas, since they were quite exposed to the solar radiation, while the surface temperature on the back of the hip and back didn't show much change, since they received no heat from the solar radiation. The reason why the surface temperature at the measurement points under the influence of solar radiation shifted periodically was that the louvers periodically block the solar radiation, and create shadows. We saw this louver affect at every point which received heat from the solar radiation.

STUDY OF SUBJECTIVE EXPERIMENT

This research was to understand the thermal environment surrounding the human body in an environment exposed to non-uniform radiant fields, so we placed a subjective experiment in an environment where solar radiation contacted the human body. According to the resulting measurements on the subjective experiment, the temperatures of those body parts that received heat directly from solar radiation were higher than those parts that did not receive heat. This proves that solar radiation has a significant impact on human body. From here on, we will discuss the CFD analysis in comparison to the results of the measurements taken on the subjective experiment.

COUPLING METHOD

This study makes use of the 65MN model incorporating CFD business use software code STAR-CD/ver.4.14.003, with some user functions. See Fig.5 for the conceptual diagram of the 65MN model. Each layer takes the balance amount of

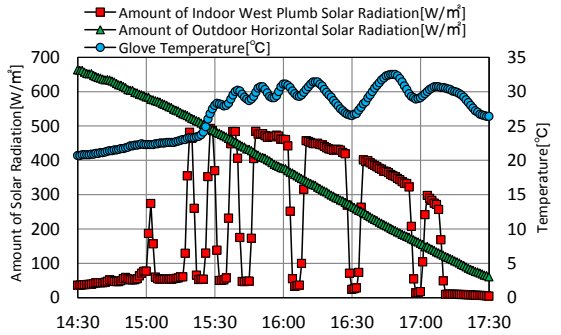

Fig.4 Glove Temperature and Amount of Solar Radiation

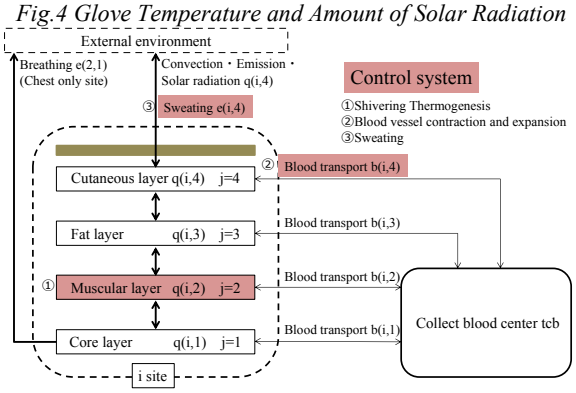

Fig.5 Conceptual diagram of the 65MN model

Tab.1 How to Expand of Latent Heat

(a)Volume Change of a Physical Quantity

$$qb(i,4)(Org) = qb(i,4)(65MN)\left(\frac{\sum_k A_{(i,k)(Org)}}{\sum_k A_{(i,k)(65MN)}}\right)^{1.5} \quad \ldots(1)$$

(b)Extensions to the Surface Element

$$qb(i,4,k)(Org) = qb(i,4)(Org)\left(\frac{A_{(i,k)}}{\sum_k A_{(i,k)(Org)}}\right) \quad \ldots(2)$$

(Sign) i : Segment number, k : Surface element number, qb(i,4)(Org) : Metabolic rate of present study, qb(i,4)(65MN) : Metabolic rate of 65MN, $A_{(i,k)(Org)}$: Area of the surface element of present study, $A_{(i,k)(65MN)}$: Area of the surface element of 65MN

heat [W] by the amount of heat produced q(i, j), blood transport b(i, j), heat conduction d(i, j) between the each layer. Breathing e(2, 1) is added in the core layer chest site, sensible heat loss amount q_t(i, 4) and sweating e(i, 4) is added to the cutaneous layer. Further collect blood center in all sites are obtained by the blood balance amount [W] of the layer. In addition, c(i, 4) is heat capacity [Wh/°C]. Sensation of heat and cold are represented by the control system, and they are calculated from the sum and difference of the set point temperature that are set in advance. Control reaction are three, they are blood vessel contraction and expansion, sweating, shivering thermogenesis.

In this study, the 65MN model was extended in order to understand to the effect of solar radiation on the localized heating of the human body. For this purpose, a numerical model of the body with elements of the outer surface was configured. Tab.1 shows the increase in *qb* metabolic rates. The

expansion method is similar to that referenced (e.g. Ozeki et al., 2004). That is, in a shape model of the human body each site, we corrected by the volume change rate ((each part surface area $A_{(org)}$) in a numerical model of the human body/surface area $A_{(65MN)}$) of the portion defined by the 65MN model corresponding)) to the surface are of each. Furthermore, the surface elements that make up a shape model of the human body each site, the physical and physiological quantities corrected every part were distributed according to the area rate. However, for volume of blood flow of the skin due to thermoregulation and radiation amount due to sweating, taking into account the influence of the local by evaluating the surface element for each control signal.

As shown in reference (e.g. Fujinaga et al., 2007), the solution to the equation of water vapor transport is coupled, however in this report we used equation 3 to calculate the water vapor saturation partial pressure.

$$psks = 0.1333 \times e^{(18.6686 - 4030.183/(t_s + 235.0))} \quad \ldots(3)$$

psks:Water Vapor Saturation Partial Pressure [kpa]、
t_s:body surface temperature [°C]

Furthermore, referring to the body surface temperature t_s value for each component's outer surface, we were able to determine the trend for each component of the outer surface.

ANALYSIS SUMMARY

Analytical Model

The experiment with the subjective experiment was conducted (2012/3/29) in a conference room (4.6×6.4×2.6m) at the Meiji University Ikuta Campus in Building A on the 10th floor, and we compared it with the CFD analysis. See Fig.6 for the analytical model. The analytical model was prepared with the window frame including the external louvers. The basic cell size was 50mm, but in the vicinity of the wall surfaces, the cell size was subdivided to 0.5mm. For the numeric values of the body model (e.g. Ito et al., 2006) used a publicly available mesh of a seated male (height:1.74m, body surface area:1.75m^2).The subjective experiment had a height of 1.75m and a body surface area of 1.76m^2 so it was scaled to approximately the same level using the DuBois equation. Fig.7 shows the mesh system used for this study. In this study, a four level layer mesh was used for the body surface. In order to minimize calculation errors in the outer gap around the body, a trim mesh, coupled with a hexa mesh, was used instead of a tetra mesh. The body surface mesh has 15,577 cells, the surrounding area has about 6,400,000 cells.

Analytical Method

For the turbulence model, we adopted Low Reynolds Number *k-ε* (e.g. Lien et al., 1966), the SIMPLE (static) computational algorithm, temperature, and *k* well as *ε* for MARS. Buoyancy modelling was used Viollet type. As for the emission analysis, a discrete

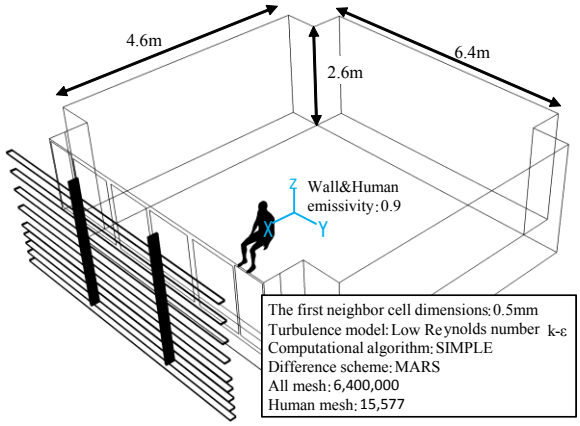

Fig.6 Analytical Model

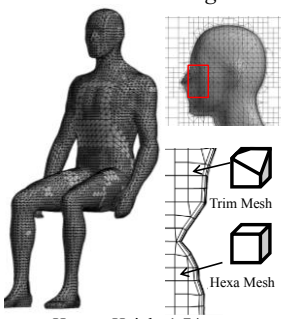

Fig.7 Analysis Condition

Tab.2 Analysis Condition

	Analysis Condition
Measurement time	2012/3/29 15:30～16:30
Time for analysis	16:10～16:20
Insolation condition	Reference Table.1
Clothing condition	Long sleeve shirt(0.17clo) pants(0.02clo) sweat(0.5clo) socks(0.2clo)
	Human boundary condition
case1	Model of Fanger $q=(36.4-t_s)/0.054\cdots(4)$
case2	65MN model

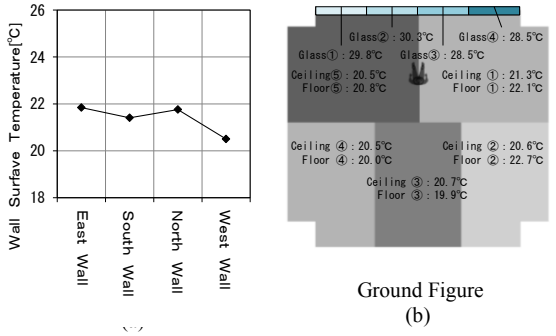

Fig.8 Wall Boundary Temperature (Average 10 Minutes)

beam was used on the human body's radiation patch for each component of the front surface. Also, the number of emission is 1024.

Analytical Conditions

The subject analysis was performed on (2012/3/29) for ten minutes (16:10～16:20) during one hour measurement period between 15:30～16:30.

For this study, we performed a static analysis of the amount of solar radiation at 16:15. The amount of direct solar radiation was 770.8 [W/m^2], the ambient solar radiation of 53.2 [W/m^2] was calculated by separating the ambient radiation on all horizontal surfaces from the direct solar radiation. Also, considered were the sun's elevation of 22.9 [°], its azimuth of 76.8 [°], and a ratio of 0.59 for solar radiation transmitted into the room by the glass facing directly west. For this study, in addition to the ambient solar radiation, we analyzed the scattered light.

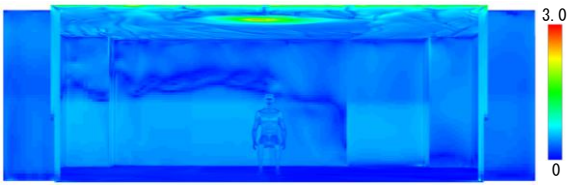

Fig.9 Distribution of y^+ [-]

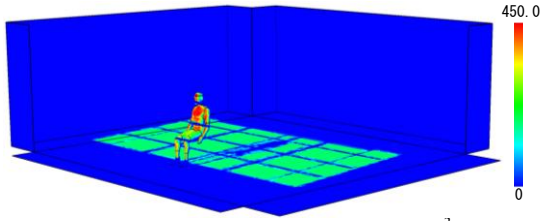

Fig.10 Direct Solar Radiation [W/m^2]

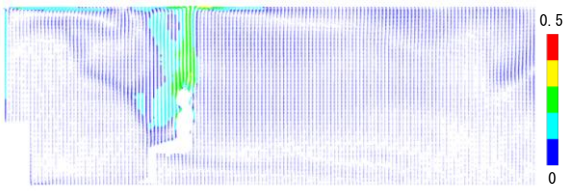

Y Section (Y=0)

Fig.11 Scalar Wind Speed of Section Plane [m/s] (Case2)

Y Section (Y=0)

Fig.12 Air Temperature of X Plane [°C] (Case2)

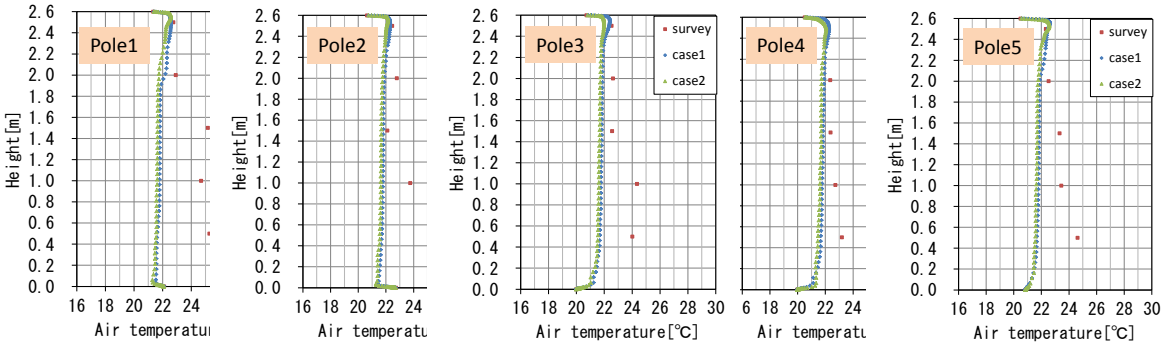

Fig.13 Profile of Air Temperature (Case2)

We analyzed the human body boundary conditions for two different cases. For Case1 we used the Fanger model, and for Case2 the 65MN model analysis. For the water vapor pressure $P_{a,ref}$=1500 [Pa], we used the Fanger model formula (4) for the analysis.

$$q = (36.4 - t_s)/0.054 \ldots (4)$$

q:sensible heat loss value [W/m^2]
t_s: body surface temperature [°C]

For the 65MN model, we analyzed the change in physiological values in proportion to core temperature. For the Fanger model analysis, we assigned a fixed value of 36.4 [°C] and a thermal resistance value of 0.054 [m^{2}K/W] (when naked). For values with clothing see reference of Air Conditioning Sanitation Engineering Association in Japan, for the survey with the body in a clothed condition, clothed thermal resistance values were established (Tab.2). The solar radiation absorption ratios were established as follows for long sleeves (black) 0.9, trousers (gray) 0.8, and skin (flesh colored) 0.7.

At the time of subject analysis, we observed thermal scattering in the surface temperature of the human body as an effect of the louvers. In this report, the produced temperature change of greater than 10 [°C] on the front pelvis and the front of the left lower leg, were outside the CFD analysis comparison target. This was the first step in verifying evidence of the usefulness of CFD analysis compared with static calculations, but analyzing whether this is atypical or normal is a subject we plan to consider later.

Fig.8 shows the boundary condition analysis used for the wall surface temperature (10 minutes interval average values). Regarding the floor, ceiling, and glass, because of the 1～2 [°C] extent of variance in measurement point temperatures, partitioning the wall surface boundaries established the temperatures shows in Fig.8-(b).

ANALYSIS RESULTS

Dimensionless Wall Range y+

When using Low Reynolds Number k-ε for the turbulence model, it is necessary to put a sufficiently fine computational mesh in the vicinity of the wall surfaces, to sufficiently reduce the wall fast mesh of y+. Fig. 9 shows the resulting dimensionless wall range of y+. The human body, as well as the wall surfaces, were without exception, less than 1. In the neighborhood of the ceiling, particularly the part above the human body, they ranged up to a value of 3.

Amount of Direct Solar Radiation

Fig. 10 shows a distribution diagram of the amount of direct solar radiation. Looking at the chest, this extends to 450 [W/m^2]. With the amount of direct solar radiation of 770.8 [W/m^2] and the radiation transmission ratio of the glass being 0.59, in general the correct analysis results were obtained. Furthermore, given the floor surface, the louvers, and

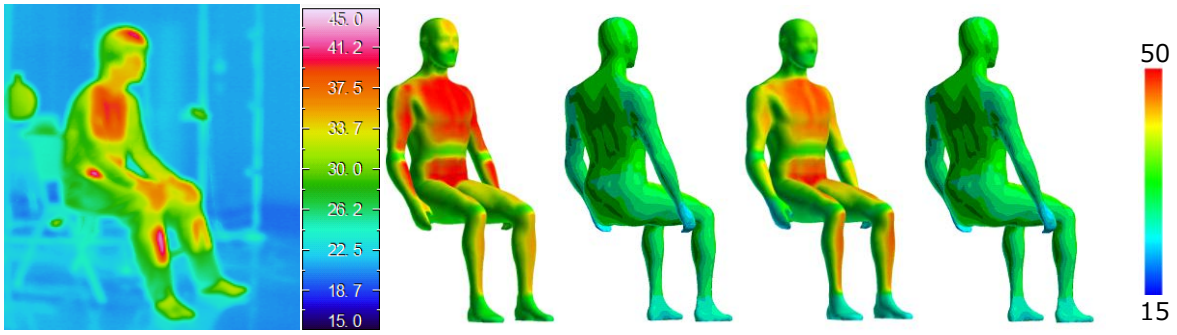

Fig.14 Distribution Body Surface Temperature [°C]

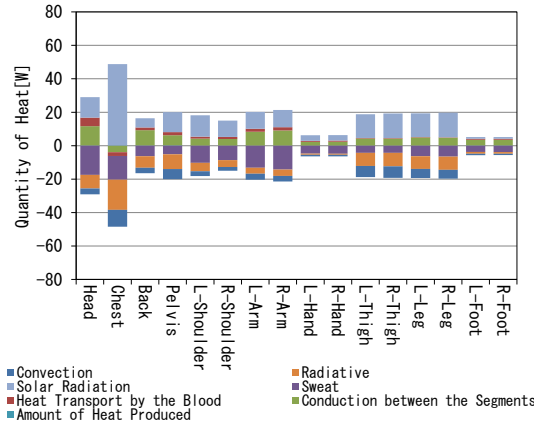

Fig.15 Heat Balance of Body Surface [W] (Case2)

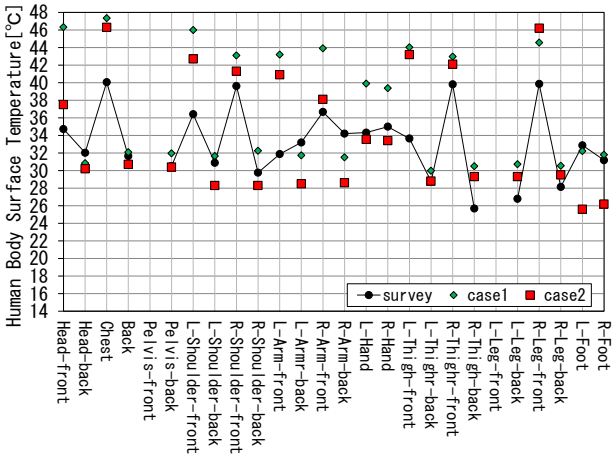

Fig.16 Body Surface Temperature [°C]

the effect of the window frame solar radiation screening, the distribution of the amount of solar radiation is correct.

Wind Speed Scalar Distribution

Fig.11 shows Case2 where Y=0, the distribution of the wind speed in the section plane. The majority fell in the distribution range of 0.1 [m/s], thus the air temperature boundaries are relatively calm. However, in the area above the human body, the air current distribution is in the neighborhood of 0.5 [m/s]. This is considered to be caused by the heat plume generated around the human body.

Central Section Plane Temperature Distribution

Fig.12 shows Case2 where Y=0, the distribution of temperature in the section plane. This yields the effect of solar radiation in the room on temperature distribution from top to bottom. Again, the heat generated by the body can be seen rising in the neighborhood of the body and above it.

Air Temperature Profile

Fig.13 shows the analytical as well as actual measurements, for Case1 and Case2, it gives the actual top to bottom temperature profiles for poles 1 through 5. It is assumed the same as those shown in Fig.2 the pole number. Looking at the temperature variance distribution from top to bottom, for both Case1 and Case2, the measured values for all the poles show large values. These are actual measurements, however the cause is thought to be due to the aluminum foil cylinder surrounding the thermocouple having an unavoidable effect on the thermal radiation measurements. Future, we need to research surveying the air temperature that is below the solar radiation boundary.

Body Surface Temperature Distribution Diagram

Fig.14 shows a thermal image as well as a distribution diagram of the analysis results for human body surface temperature. For both Case1 and Case2, the body temperature distribution tendency due to the louvers and the window frame can be observed. Furthermore, in Case1, all body surfaces have moved to the vicinity of 45 [°C]. But, comparing Case2 with Case1, we get a temperature distribution chart that trends closer to actual measurements.

Body Surface Heat Balance (Case2)

Fig.15 shows the heat balance quantities of body surface for Case2. Looking at the solar radiation heat quantities, those near the chest have a large value. Also, at all positions, sweating accounts for a large proportion of the thermal radiation.

Body Surface Temperature

Fig.16 shows the actual surface temperature instrumentation measurements from the survey for each location and the analytical results. Looking at the analytical results, the trend due to the presence or absence of solar radiation on the front and rear of the human body, and that of the survey, gives identical results. Furthermore, comparing Case2 with Case1, the temperatures of the entire body are lower. However, for the temperatures of the rear parts of the body, the survey produces a disparity. It is considered that the reason why the temperature of the Case2 is lower overall than in Case1, it is considered the effect of sweating in Case2, the temperature is lowered in the entire human body.

CONCLUSION

Within the boundaries of the solar radiation, values using a subjective experiment were compared in order to evaluate the usefulness of combining the body thermoregulation model with CFD analysis. As a result, by means of expanding 65MN model to each outer surface component, we acquired an understanding of the effect of localized solar radiation on the functioning of body thermoregulation. Also, comparing the 65MN model with the Fanger model for areas impacted by direct solar radiation, we were able to get actual measurements that closely matched the calculated results. However, because the sun position changes, solar radiation is in the dynamically phenomenon. Therefore, we performed static analysis as the first stage of the usefulness of verification this time, it is necessary to advance the analysis to account for the dynamically in order to perform the detailed analysis within the boundaries of the solar radiation. After this, via CFD analysis, we plan to evaluate the effectiveness of various solar radiation screening techniques.

REFERENCES

Fujinaga, Shiraishi, Tanabe: Investigation Relating to 65MN Model and CFD Coupling Analysis (3rd Edition) Human Body Model Extension from Each Component to Surface Components, Architecture Institute of Japan Research Report. Kyushu Branch, pp.385-388, 2007

Ito, Horita: Preparing a Numerical Analysis Using the Visual Mannequin Grid Library, Air Conditioning Sanitation Engineering Association Collected Papers (Engineering Article), No133, pp. 27-34, 2006

Lien, F,S., Chen, W.L., Leschziner, M.A. : Low-Reynolds-Number Eddy- Viscosity Modeling Based on Non-Linear Stress-Strain/Vorticity Relations, Engineering Turbulence Modeling and Experiments 3 pp.91-100, 1966

Ozeki, Tanabe: Solar Radiation Boundary for Human Body Thermoregulation 65MN model Tepid Skin Survey and Subjective Experiment Results Comparison, Architecture Institute of Japan Program Series Collected Articles Volume 581, pp.29-36, 2004

Tanabe, Nakano, Kobayashi: Investigation Concerning a 65 Partition Heat Boundary Evaluation Model, Architecture Institute of Japan Program Series Collected Articles Volume 541, pp.9-16, 2001